Heliyon 11 (2025) e42695

Contents lists available at ScienceDirect

Heliyon

journal homepage: www.cell.com/heliyon

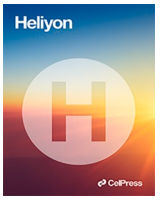

Research article

A specific model of resting-state functional brain network in MRI-negative temporal lobe epilepsy

Xue Yang [a,*], Manling Ge [b], Shenghua Chen [b], Kaiwei Wang [a], Hao Cheng [a], Zhiqiang Zhang [c]

[a] School of Life Science and Health Engineering, Hebei University of Technology, Tianjin, China
[b] Hebei Province Key Laboratory of Electromagnetic Field and Electrical Apparatus Reliability, Hebei University of Technology, Tianjin, China
[c] Department of Medical Imaging, Clinical School of Nanjing University School of Medicine (affiliated to Jinling Hospital), Nanjing, China

ARTICLE INFO

Keywords:
Resting-state fMRI
Functional brain network
MRI-negative temporal lobe epilepsy
Specific FC model
Machine learning

ABSTRACT

Purpose: Without any visible indicator on structure magnetic resonance imaging (MRI), the diagnosis of MRI-negative temporal lobe epilepsy (NTLE) gets harder. By considering healthy control (HC), a specific functional connectivity (FC) model was constructed in a network topology to improve FC computation to a high-level.

Methods: MRI data of 20 NTLE patients and 60 HC were pre-processed. Relative to HC, a network-level specific FC model of each network index was built to score the network functions for each NTLE patient. The specific brain areas (regarded as ROIs) were extracted for NTLE by sensitivity analysis of scores. By considering scores of specific ROIs as feature vectors to input into a SVM respectively, a specific NTLE classifier was constructed. Both 10-fold cross validation and hold-out method were utilized to validate the classification and to evaluate the effectiveness of our specific FC models. Simultaneously, the specific FC model was compared to the conventional FC model of Pearson correlation.

Results: By the constructed model for specific FC at a network-level, 11 specific ROIs, such as, frontal lobe, temporal lobe, parietal lobe, hippocampus, and occipital lobe, were extracted for NTLE. Accuracy of our specific NTLE classifier could reach up nearly 93 %, over 6 % greater than conventional FC model of Pearson correlation.

Conclusions: The network-level specific FC model might provide a new methodology for machine-aiding detection of functional abnormal lesions of NTLE by resting-state functional MRI.

1. Introduction

Mesial temporal lobe epilepsy (mTLE) is a neurological and psychiatric disease with abnormal neural discharges in deep brain, leading to dysfunctions in the functional networks in the central system, even extend to the whole-functional brain networks [1]. Nearly 60 % of mTLE is MRI-positive temporal lobe epilepsy (PTLE), the typical indicator of hippocampal sclerosis could be visible on structure MRI. About 30 % is NTLE, whose clinical manifestations of mesial temporal lobe seizures [2], lower prevalence of febrile convulsions [3], and lower rates of seizure freedom after surgery [4,5]. Histopathology may be normal or show relatively mild hippocampal neuronal loss, and the temporal neocortex is either normal or some shows subtle dyslamination [6]. Taken together,

* Corresponding author.
E-mail address: 202232902022@stu.hebut.edu.cn (X. Yang).

https://doi.org/10.1016/j.heliyon.2025.e42695
Received 17 January 2024; Received in revised form 11 February 2025; Accepted 12 February 2025
Available online 13 February 2025

symptoms of NTLE seizures appear similar to those of PTLE, and explore functionally abnormal lesions of NTLE seems more difficult than that of PTLE, these phenomena have suggested that different brain networks may be affected and related cognition may be impaired in NTLE [7], implying that the functional biomarkers could provide potential signs for it.

At present, the advantages of resting-state fMRI are becoming more and more prominent in epilepsy. With its noninvasive, fast, high spatial resolution, good adaptability and comfortable experience for a patient, rfMRI has become an advanced technology. More and more scholars are applying complex network theory to rfMRI, using brain functional connectivity technology to construct and analysis brain functional connectivity networks from multiple perspectives, discovering topological attribute relationships between network nodes, and investigating the integration and separation mechanisms of brain functions from the perspective of a system level [8,9]. The imaging index is expressed as functional connectivity (FC). In PTLE, it was demonstrated that the abnormal discharges would affect the FCs in some brain area, such as hippocampus, contralateral mesial temporal and default mode network et al., which provided an important basis for detecting the brain dysfunction [10]. However, the significant abnormality of the FCs hasn't be clear yet in the network of NTLE. The main cause to affect the imaging quality might be the FC computing, e.g., Pearson correlation algorithm, which is operating at a low-order level.

Functional network analysis is a high-level FC computation based on graph theory [11,12]. In recent years, the International League Against Epilepsy (ILAE) emphasizes the concept of epileptic brain network to formulate the classification criteria of epilepsy [13,14]. For example, the classification predicted the response of children with epilepsy to the anti-epileptic drugs at a single network index, such as degree centrality [15]. Now, combination of network-level FC computing and machine learning is a popular analysis tool, especially, the multiple network indexes fusion technology is being integrated to improve the imaging quality [16]. Additionally, the connectome data analysis is helpful, such as, the epilepsy laterality might be localized by the extra-hippocampal radiomics analysis on the patients with NTLE [17].

Taken together, a network-level specific FC model under complex network theory is constructed to find the functional imaging indicators for a single NTLE patient, relative to the healthy people, for purpose of improving the FC computing to a high level. To validate our model, the classification rate by SVM would be employed. Example of 20 NTLE and 60 HC, the work flowchart is shown in Fig. 1.

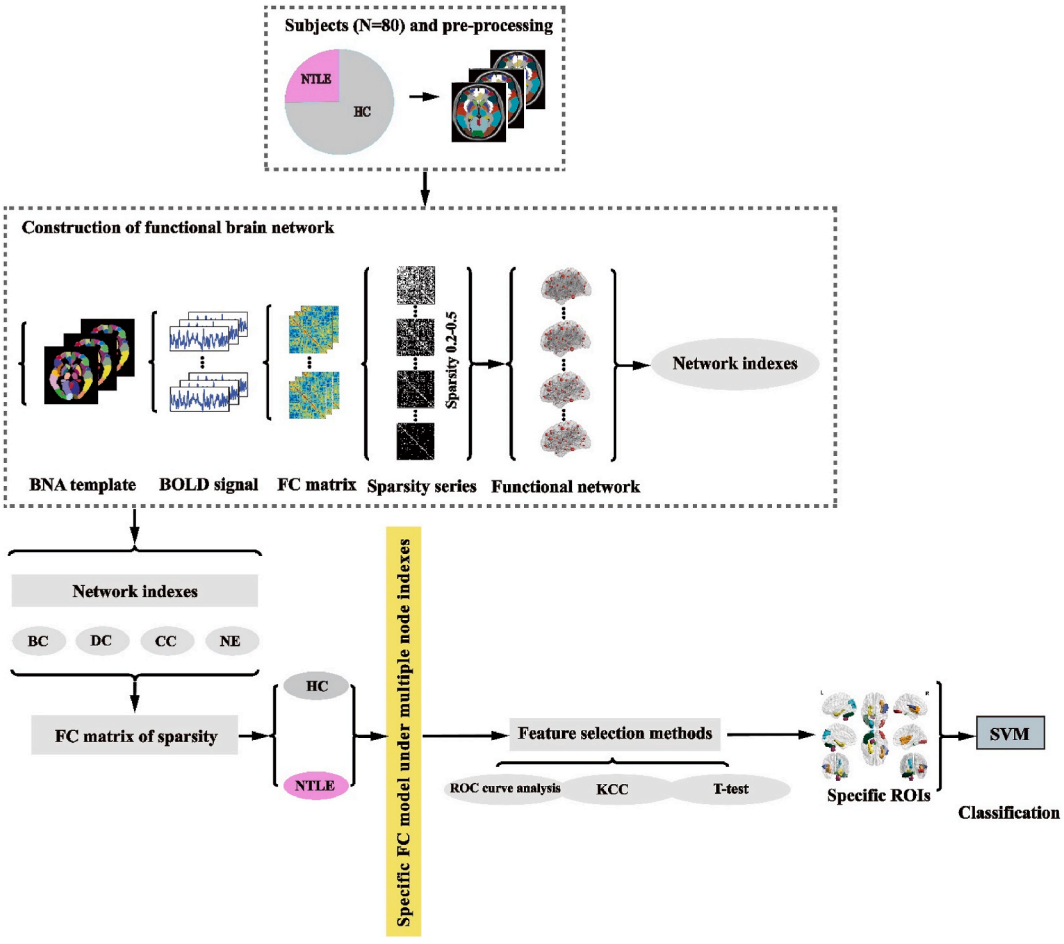

Fig. 1. Methodology flowchart for this study.

2. Materials and methods

2.1. Materials

2.1.1. Data acquisition

The rfMRI data of 20 patients with NTLE, and 60 healthy people were collected from Jinling Hospital of Medical College in Nanjing University. All subjects were scanned by 3.0T Siemens Trio MRI scanner in the hospital, with same parameters: repetition time (TR) = 2000 ms, echo time (TE) = 30 ms, flip angle (FA) = 90°, matrix size = 64 × 64, scanning field of vision (FOV) = 240mm × 240 mm, layer thickness = 4.00 mm, and layer spacing = 0.40 mm. Our study was approved by the Medical Ethics Committee of the hospital and all subjects signed the informed consent, whose information was labeled in Table 1.

All patients meet the following inclusion criteria: i) meet the criteria of the International League for the Diagnosis of Epilepsy and are diagnosed with medial temporal lobe epilepsy type; ii) Subjects aged between 19 and 38 years old; iii) No contraindications for MRI scans such as intracranial metal implants; iv) Normal mental state, able to cooperate and communicate normally, with normal cognitive function; v) All patients with temporal lobe epilepsy showed no significant structural loss on structural MRI scans. Among them, those who can observe hippocampal structural lesions on structural MRI are referred to as PTLE, while those who cannot are referred to as NTLE.

2.1.2. Data pre-processing

The rfMRI data were pre-processed by the toolkit of FMRIB software library in Harvard Medical College, USA and quality-inspected by the Laboratory for the study of the Brain Basis o Individual Differences in Harvard Medical College, USA on Intel Xeon Sliver 4112 × 16, 64cores CPU, operating system Centos 7.6 processing platform, in Martinos Medical Imaging Center of Harvard Medical College, USA [18,19]. The processing algorithm flow and quality detection (with the head motion control of 0.2 mm) were necessary. The pre-processing time of each subject was about 15h.

At first, the following steps were conducted: (1) after the first 4 time points was removed, the time-layer correction was done by the SPM2 software, and body translation and head movement were corrected by the FSL software; (2) average signal of the whole brain was normalized, and data space was standardized to a voxel size of 2 mm as well as registered to the MNI (Montreal Neurological Institute) standard space; (3) data were band-pass filtered at a frequency band of 0.01Hz–0.08Hz.

Then, the pre-processed data were projected to the Brainnetome Atlas (BNA), including 246 brain areas [20]. As a consequence, the 4-D spatiotemporal data of the BOLD signals including 3-D space coordinates of 246 brain areas and 1-D time series were formed. The work was performed by Inter Core i9-9900K, 64cores CPU, independent display card NVIDIA RTX 2060, operating system Windows10 processing platform, the processing time is about 23 min. By the software of DPABI V4.3 [21], a 480s time course of BOLD signals, including 246 time-points was prepared for the post-processing, with 246 encephalic regions.

2.2. Functional brain network

2.2.1. Network construction

Under the small-world attributes in graph theory [22,23], the functional network was constructed in a topology made of 4 local network indexes for each subject.

(1) Node

By considering each brain area as a node, and its index value was regarded as the average time series over all voxels in this area, a total of 246 nodes were formed.

(2) Edge

The edge is the connection intensity between nodes for each subject. Here, it was estimated by the static FC such as Pearson correlation coefficient, which was [−1, 1]. Taking the BOLD signals between two areas as an example, when the correlation coefficient of two time series is [0, 1], denoted as positive correlation, indicating two BOLD signals showed the functional synergy. In reversal, when [−1, 0], denoted as negative correlation, indicating the functional antagonism. When 1, indicating completely correlated or autocorrelated, while, when 0, completely uncorrected. The greater the absolute value is, the stronger the FC, and verse vice. Here, a 246 × 246 matrix of the FCs were constructed and after the FCs matrix were average over column or row, a total of 246 edges were

Table 1
Information of all subjects.

Group	Number of subjects	Sex		Age/years
		Male	Female	
NTLE	20	9	11	26.70 ± 4.41
HC	60	27	33	26.62 ± 5.51

formed at all nodes.

(3) Sparsity and network construction

In the constructing a network, the FCs matrix were divided by the threshold to generate a binary adjacency matrix. If a matrix element was greater than the threshold, it was set to be 1, otherwise 0. Therefore, the threshold setting would directly determine the generation of edges in the network, which has an important impact on the network scale and topological structure. As the threshold was increased, the number of edges would also increase monotonously, but not necessarily linearly. The sparsity is generally used to set the threshold, that is, the ratio of the actual number of edges in the network to the maximum number of edges that may exist in the network. Because the small world property in functional brain network would tend to be randomized, the default sparsity is generally less than 0.5 [24]. In general, the sparsity is 0.05–0.5 with a 0.05 step to threshold the FCs matrix in a network construction. However, there might be invalid values of network parameters in the first 3 sparsity levels e.g., 0.05, 0.10 and 0.15, thus, a total of 7 sparsity levels were employed among 0.2 to 0.5 by the open software GRETNA (http://www.nitrc.org/projects/gretna/).

2.2.2. Topological properties of functional network

There were two kinds of topological properties in the functional network: local properties and global properties [25]. Network features of nerve and mental diseases were represented by the local attributes. These local attributes were depicted by the network indexes, such as betweenness centrality (BC), degree centrality (DC), clustering coefficient (CC) and node efficiency (NE) [26]. For each subject, the 7 × 246 matrix of sparsity sequence were formed and averaged over the sparsity levels.

2.3. A network-level specific FC model

2.3.1. Specific FC model of network index

A specific FC model of each network index (specific index, denoted as SI) was constructed to score a FC in a brain network of a single NTLE patient, relative to HC people, for purpose for improving the FC computation of Pearson correlation to a higher level. The SI model was in formula (1):

$$\mathrm{SI}_{s,i} = \frac{1}{\mathrm{N\text{-}1}} \sum\nolimits_{p=1,p\neq s}^{N} \left(1\text{-}\mathrm{corr}\left(r_{s,i}, r_{p,i}\right)\right) \tag{1}$$

In formula (1), r_i is the FCs vector of a network index in the *i-th* brain area estimated by Pearson correlation, $r_{s,i}$ is that of the *s-th* NTLE patient, while, $r_{p,i}$ is that of the *p-th* HC people, N is the HC number, therefore, $SI_{s,i}$ is the specific index of the functional brain network node between the *s-th* patient and the *i-th* brain area of all HC people. In the HC people, $SI_{s,i}$ is the specific index of the functional brain network node between the *s-th* HC person and the *i-th* brain area of all HC people excluding the *s-th* HC.

To compare the differences in SI between NTLE patients and HC people, the SI standardization was conducted by measuring relative position of the SI value of a network index of a NTLE patient in the HC distribution [27]. The specific FC model was defined by the standardized SI (denoted as SSI) in formula (2):

$$\mathrm{SSI}_{s,i} = \frac{1}{\mathrm{std}_{\mathrm{SI}_{s,i}}} \left(\mathrm{SI}_{s,i}\text{-}\mathrm{mean}_{\mathrm{SI}_{s,i}}\right) \tag{2}$$

In formula (2), mean_SI_i denotes the mean value of SI in the *i-th* brain region for 60 HC, and std_SI_i denotes the standard deviation of SI in the *i-th* brain region for 60 HC.

As a consequence, the 20 × 246 and 60 × 246 standardized SSI matrices of a network index were formed for the NTLE group and HC group, respectively.

2.3.2. Specific features extracted by our model for NTLE (specific ROIs)

By the specific FC model of each network index, the features of 246 brain regions can be extracted for NTLE group or HC group respectively. In order to get rid of the redundant information caused by the extraction algorithm, reduce the feature dimension and avoid the randomness caused by a single feature selection method, here, three algorithms, such as receiver operating curve (ROC), Kendall tau rank correlation coefficient (KCC) [28] and *t*-test for independent samples between groups were employed to extract the functional imaging bio-markers specific for NTLE. Only the specific brain area to fit simultaneously three algorithms of a network index can be regarded as a functional imaging bio-marker, denoted as a specific ROI, that would be visualized by the software BrainNet-Viewer (https://www.nitrc.org/projects/bnv/).

(1) ROC

A sensitivity analysis of SSIs was conducted by the ROC curve and the area under ROC curve (AUC value) to extract the features between NTLE group and HC group. The larger AUC, the stronger the significant sensitivity would be, and vice verse.

(2) KCC

KCC is suitable for a large-scale feature selection, such as whole brain analysis. KCC can extract the features by measuring the relevance of each feature represented by SSI in a distribution free test of independence between two variables. Assuming that a two-observation dataset $\{x_{ij}, y_j\}$and $\{x_{ik}, y_k\}$ represents for samples in the HC group and in the NTLE group respectively. x_{ij} is the *i-th* SSI feature of the *j-th* sample in the HC group and y_j is the class label for HC (+1). Similarily, x_{ik} is the *i-th* SSI feature of the *k-th* sample in the NTLE group and y_k was the class label for NTLE (−1). For a pair of two-observation dataset, the concordance between the feature pair is determined by the following formula (3) and (4):

$$\mathrm{sgn}\left(\mathrm{x_{ij}\text{-}x_{ik}}\right) = \pm \mathrm{sgn}\left(\mathrm{y_j\text{-}y_k}\right) \tag{3}$$

where, '+' indicates concordant feature pair, '−' indicates discordant feature pair.

Given *m* samples in the HC group and *n* samples in the NTLE group, the KCC of the *i-th* SSI feature can be defined as the below:

$$\mathrm{KCC_i} = \frac{\mathrm{n_c\text{-}n_d}}{\mathrm{m \times n}} \tag{4}$$

Obtained from formulas (3) and (4), n_c and n_d are the number of concordant and discordant pairs respectively, and a total number of sample pairs is $m \times n$. The value of KCC is [−1,1], and the discriminative power was defined as the absolute value of KCC. The larger the absolute value, the greater the categorical discrimination between NTLE patient group and HC group.

(3) T-test

The *t*-test corrected by false discovery rate (FDR) for independent samples between groups ($p_{FDR} < 0.05$)shows the significance.

2.3.3. Specific network features fusion

The serial SSIs fusion of four network indexes in the specific ROIs, were considered as the feature vectors [29], denoted as $\mathrm{SSI_{fusion}}$ in formula (5):

$$\mathrm{SSI_{fusion}} = [\mathrm{SSI_1}, \mathrm{SSI_2}, \mathrm{SSI_3}, \mathrm{SSI_4}] \tag{5}$$

where, SSI_i is the specific score estimated by a network index.

2.4. Conventional FC model

In order to emphasize the advantages of the network-level specific FC model, the conventional FC model of Pearson correlation is used for experimental verification. The conventional FC model construction method was performed as following: Calculate Pearson correlation matrix (FC matrix) of the subjects after matching BNA atlas; The FC matrix of each subject is averaged. Then, NTLE and HC groups respectively get a set of 20 × 246 feature matrices and a set of 60 × 246 feature matrices, which are used for feature selection.

2.5. Specific features tested by machine learning

Support vector machines (SVM) [30] was employed to classify the patients from the healthy people in case of the small sample size. According to linear inseparability, SVM uses kernel function to map the input variables into a high-dimensional feature space, where the optimal classification hyperplane is constructed. Here, NTLE classifier based on SVM was constructed, denoted as a specific NTLE classifier, and the SSI values of network indexes respectively in specific ROIs was considered as feature vectors input into NTLE classifier. In addition, in order to avoid over-fitting and randomness in the process of classification verification, the 10-fold cross validation were employed in the validation for the classification accuracy by SVM. Average classification rate could validate the precision of a FC computation, e.g., our network-level specific FC model and conventional FC model of Pearson correlation respectively.

Compared to other cross-validation methods, the hold-out method has no influence of random factors in the experimental process. The validation split the dataset into two mutually exclusive sets, one as the training set and the other as the test set. The experiment was repeated by using a number of random divisions and the average value was taken as the evaluation of the hold-out method. Moreover, random cross validation can avoid overfitting of experimental results. In the 10-fold cross validation, 42 subjects were randomly selected as the training set, and the rest of 18 subjects were used as the test set (the proportion of training set and test set was fixed at 7:3).

3. Results

3.1. Specific bio-marker areas for NTLE

After three feature extraction algorithms were performed by multiple network indexes fusion ($\mathrm{SSI_{fusion}}$) between NTLE and HC, the functional bio-marker areas were extracted shown in Fig. 2, and the significance values were labeled in Table 2. In Fig. 2A and D, a total of 11 specific areas were respectively extracted by feature extraction methods of ROC sensitivity analysis and KCC based on our

network-level specific FC model. In Fig. 2B, the specific areas extracted by specific FC model were visualized by the software BrainNetViewer. The statistical distribution histogram of KCC values of all network indexes were shown in Fig. 2C. The KCC values of the features basically follows, a normal statistical distribution, and the features would be extracted by its middle interval where the KCC values are the greatest. It is obvious that a total of 11 features would be extracted. In Table 2, p values showed the significance ($p_{FDR}<0.05$). Taken together, a total of 11 bio-marker areas were convergent in three feature extraction algorithms. Under the specific index of BC, there were significant differences in 6 brain areas between NTLE and HC ($p_{FDR}<0.05$), and under the specific index of DC, there were 2 significant brain areas ($p_{FDR}<0.05$), and under the specific index of CC, there were 2 significant brain areas ($p_{FDR}<0.05$), as well as under the specific index of NE, there were 2 significant brain areas ($p_{FDR}<0.05$). There is a common significant brain area between the specific index of BC and CC. In summary, a total of 11 significant brain areas could be extracted by our network-level specific FC model, including superior frontal gyrus, middle frontal gyrus, middle temporal gyrus, posterior superior temporal sulcus, inferior parietal lobule, hippocampus, parahippocampal gyrus, and lateral occipital cortex, where middle frontal gyrus, inferior parietal lobule, and lateral occipital cortex showed significant differences in several node-specific metrics. The mean value of the AUC of the ROC for these features is 0.750 and the mean value of the KCC is 0.308, as shown in Fig. 2D.

In Fig. 3 and Table 3, three feature extraction algorithms were performed by the conventional FC model of Pearson correlation between NTLE and HC. In Fig. 3A and D, a total of 9 significant brain areas could be extracted by the FC model of Pearson correlation ($p_{FDR}<0.05$), including frontal lobe (2 brain regions), temporal lobe (4brain regions), parietal lobe (2 brain regions) and insular gyrus. In Fig. 3A and C, the mean value of the AUC of the ROC for these features is 0.584 and the mean value of the KCC is 0.286. In Fig. 3B, the specific areas extracted by conventional FC model were visualized by the software BrainNetViewer. Compared to the features of our network-level specific FC model, the conventional FC model of Pearson correlation had poor discriminatory power.

In Fig. 4, the SSI values of 11 specific ROIs estimated by a total of 4 network indexes for all NTLE patients and all HC people were clustered. The SSI values estimated by the network indexes denoted as BC, DC, CC and NE were respectively indicated in Fig. 4A-F, Fig. 4G-H, Fig. 4I-J and Fig. 4K-L. An obvious cluster by a total of 4 network indexes, such as BC, DC, CC and NE could be found between NTLE patients and HC people. In reversal, the FC values estimated by the conventional model of Pearson correlation in all 9 significant brain areas for NTLE patients and HC people were clustered in Fig. 5A-I. It was found that the conventional FC model of Pearson correlation had lower ability of clustering than our network-level specific FC model.

3.2. Classification and validation

In order to evaluate the effectiveness of our specific FC method at network level and the conventional model of Pearson correlation, the machine learning of SVM was employed to verify the performance of our specific FC score model and the conventional model respectively. By constructing a specific NTLE classifier, a classification was done for NTLE from HC and then was validated, thus, classification accuracy evaluated the effectiveness. The stability of the classifier was respectively verified by hold-out method and 10 times random cross validation as labeled in Tables 4 and 5.

4. Discussion

4.1. The network-level specific FC model

Considering the FCs of healthy people as a control, a network-level specific FC model was proposed under multiple functional network indexes fusion, by which the specific and unique biomarker areas for the abnormal functional activities could be extracted effectively for NTLE. The performance could be verified by machine-aided classifying the NTLE from HC, as labeled in Tables 4 and 5. Compared to the conventional FC model of Pearson correlation, the network-level specific FC model shows significantly better and more stable classification performance, in particular, in the unique features extraction.

In addition, the dimension reduction by 3 algorithms of feature extraction can effectively remove redundant features at a network level, therefore, avoid the dependence of extraction features on a certain algorithm. This may be the main cause why the NTLE classifier could sustain a high classification stability in multiple network indexes fusion. The classification accuracy of its specific features in random cross validation and hold-out method was less than 6 % the network-level specific FC model, which reflected the limitations of the conventional FC model in the study of NTLE, and also emphasized the advantages of high-level operation of the network-level specific FC model proposed by us.

4.2. Specific bio-markers for NTLE

By our network-level specific FC model, the specific ROIs for NTLE could be extracted. We found that the specific ROIs selected using three feature selection methods (ROC, KCC and T-test) focused on the hippocampus, occipital lobe, frontal lobe, temporal lobe and parietal lobe, which were converge to the biomarkers of epilepsy study in previous years. Hippocampus [31], one of the important brain regions in the potential network in epileptic seizures, which is related to advanced cognitive functions such as learning, situational memory and consciousness. Hwang et al. [32], found that the cognitive impairment of epilepsy was associated predominantly with decreased local gyrification in regions including occipital lobe. The temporal lobe is a very complex lobe of the brain, with very high-level cognitive functions of memory. The central anterior gyrus of the frontal lobe serves as the motor center, and its lesions usually manifest as convulsions or paralysis of the contralateral limb [33]. The abnormal limb movements in patients with epilepsy are closely related to the function of the parietal lobe. The tonic-clonic spasms of limbs are usually associated with abnormal discharges

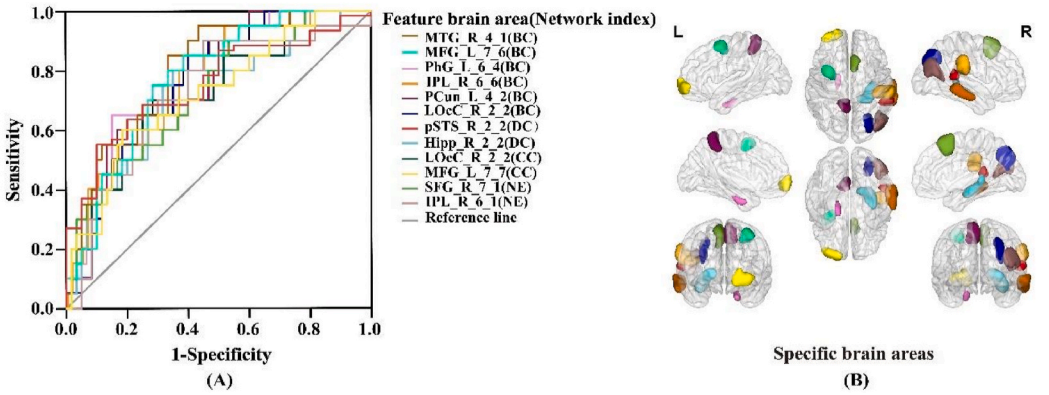

(A) (B)

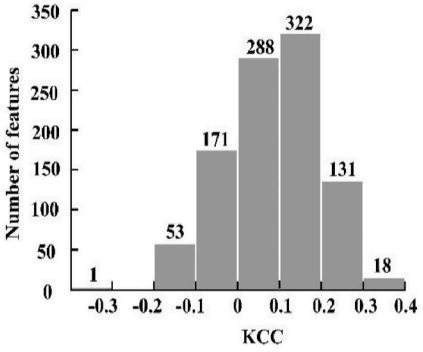

(C)

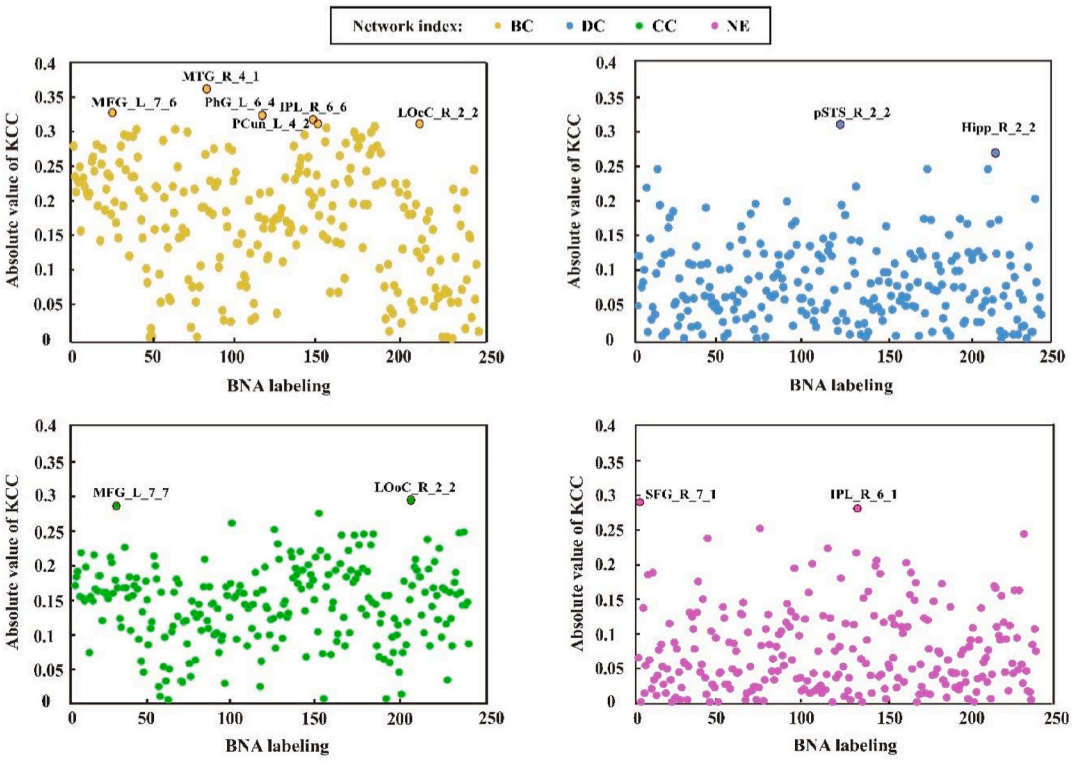

(D)

(caption on next page)

Fig. 2. Functional bio-marker areas are extracted by the specific FC model of multiple nodes indexes fusion between NTLE and HC. (A) 11 specific ROIs are extracted by the ROC curve; (B) Specific ROIs are displayed by BrainNet Viewer; (C) Histogram of KCC for all features in the network indexes; (D) Absolute value of KCC.

Table 2
Between-group significance of network indexes in 11 bio-marker areas between NTLE and HC under the specific FC model.

Bio-marker area (Network index)	BNA atlas label	Between-group mean of SSI		AUC of ROC	Absolute value of KCC	p_{FDR}
		NTLE group ($\times 10^{-16}$)	HC group ($\times 10^{-16}$)			
MTG_R_4_1(BC)	82	1.29	0.25	0.802	0.3718	0.0006
MFG_L_7_6(BC)	25	1.00	0.21	0.773	0.3369	0.0002
PhG_L_6_4(BC)	115	0.97	0.24	0.771	0.3338	0.0004
IPL_R_6_6(BC)	146	0.94	−0.23	0.766	0.3276	0.0013
PCun_L_4_2(BC)	149	0.98	−0.56	0.761	0.3215	0.0012
LOcC_R_2_2(BC)	210	0.68	0.13	0.761	0.3215	0.0121
pSTS_R_2_2(DC)	124	−0.85	−0.55	0.752	0.3102	0.0011
Hipp_R_2_2(DC)	218	0.70	0.16	0.717	0.2681	0.0066
LOcC_R_2_2(CC)	210	0.87	−0.18	0.728	0.2804	0.0013
MFG_L_7_7(CC)	27	0.75	0.63	0.722	0.2732	0.0038
SFG_R_7_1(NE)	2	0.80	−0.35	0.728	0.2804	0.0021
IPL_R_6_1(NE)	136	0.71	0.46	0.721	0.2722	0.0073

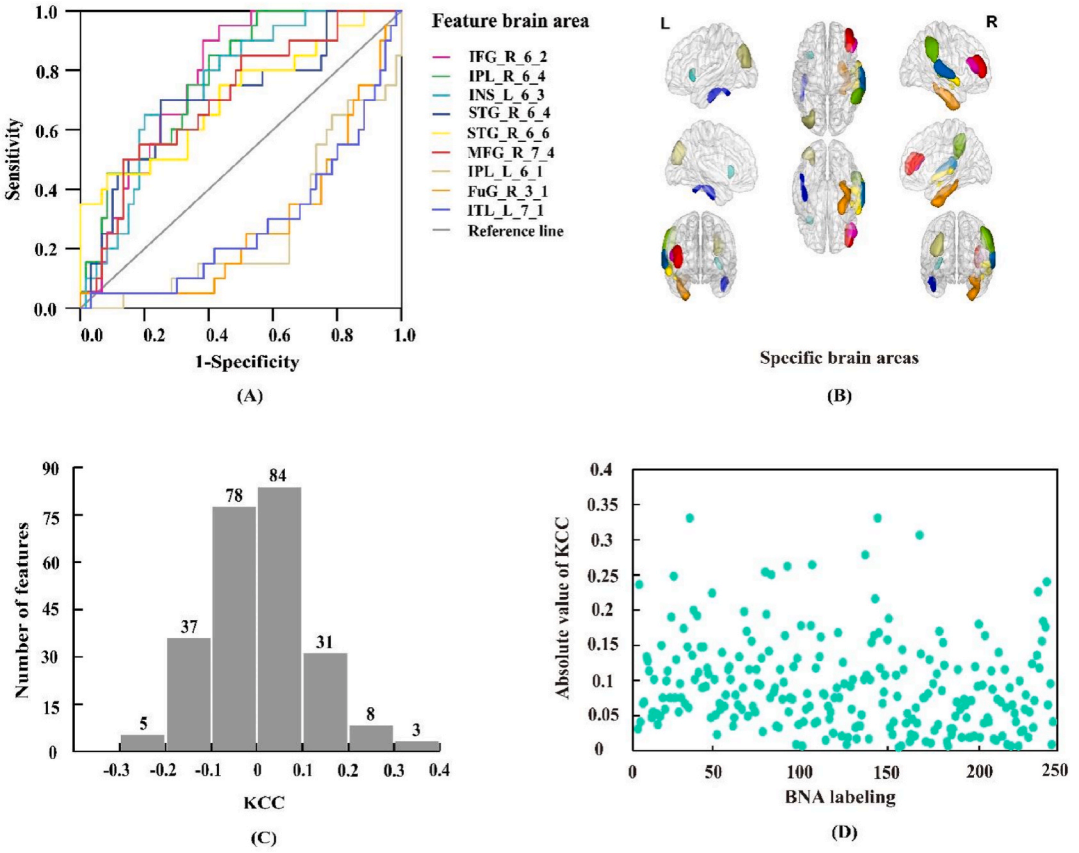

Fig. 3. Functional bio-marker areas are extracted by the conventional FC model between NTLE and HC. (A) 9 specific ROIs are extracted by the ROC curve; (B) Specific ROIs are displayed by BrainNetViewer; (C) Histogram of KCC for all features in the network indexes; (D) Absolute value of KCC.

from the lower region of the parietal lobe [34]. Temporal lobe epilepsy is a complex network disease. At the structural level, the results of this study are consistent with it. Functional disruption of temporal lobe epilepsy at the brain region level was revealed, which may provide novel insights for any potential diagnostic and therapeutic approaches.

Table 3
Between-group significance of network indexes in 9 bio-marker areas between NTLE and HC under the conventional FC model.

Bio-marker area (Network index)	BNA atlas label	Between-group mean of SSI		AUC of ROC	Absolute value of KCC	p_{FDR}
		NTLE group ($\times 10^{-2}$)	HC group ($\times 10^{-2}$)			
IFG_R_6_2	32	3.84	1.19	0.774	0.3379	0.0001
IPL_R_6_4	142	1.85	−0.88	0.774	0.3379	0.0004
INS_L_6_3	167	5.09	2.96	0.753	0.3122	0.0013
STG_R_6_4	76	4.95	2.88	0.710	0.2588	0.0038
STG_R_6_6	80	2.95	1.21	0.707	0.2547	0.0022
MFG_R_7_4	22	1.77	−0.16	0.705	0.2527	0.0110
IPL_L_6_1	135	−2.64	−0.49	0.269	0.2845	0.0005
FuG_R_3_1	104	1.95	3.49	0.282	0.2691	0.0203
ITG_L_7_1	89	1.00	2.81	0.284	0.2660	0.0058

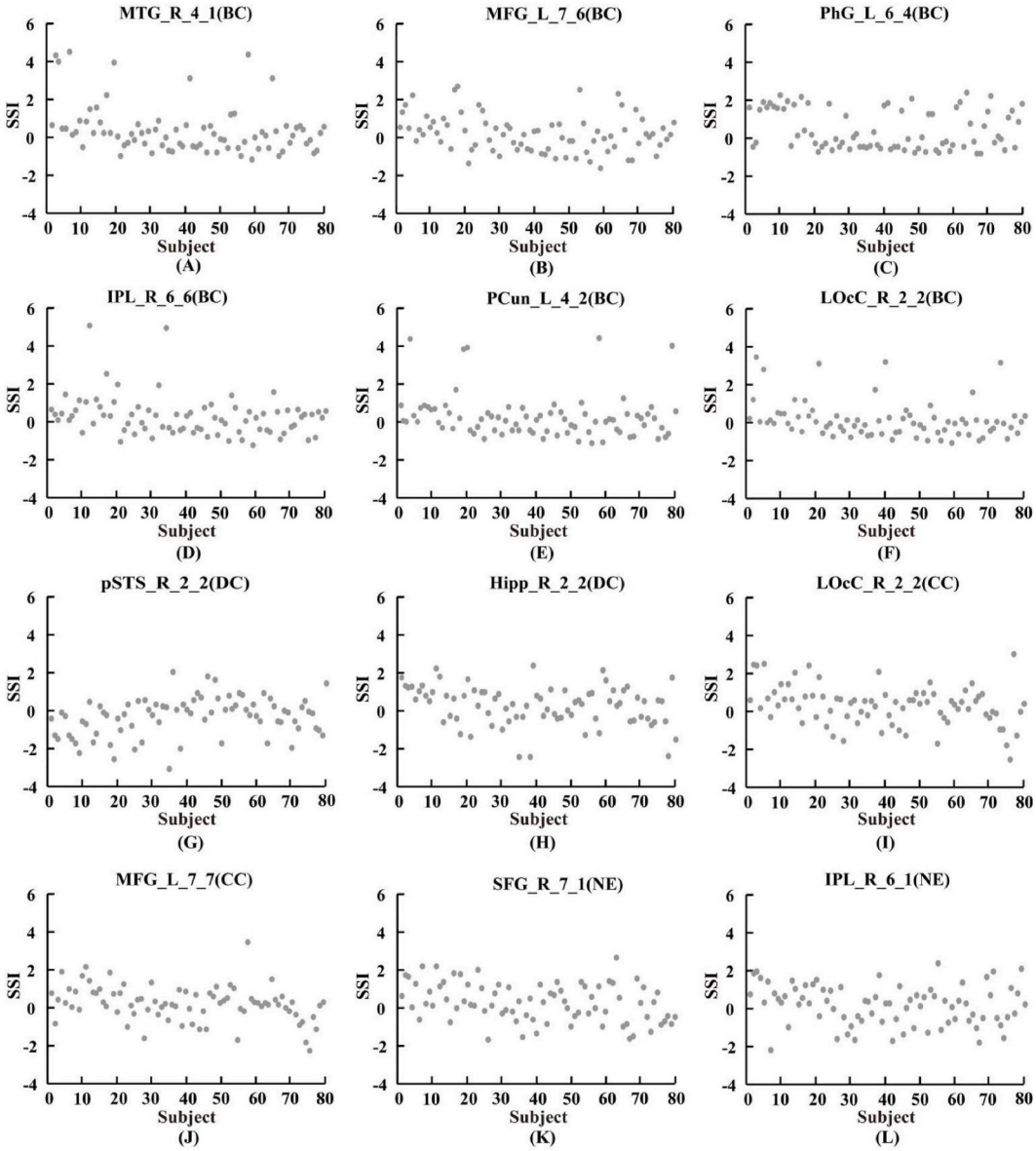

Fig. 4. Cluster of SSI values at the specific ROIs for NTLE and HC under the specific FC model, the first 20 subjects are NTLE,and the last 60 subjects are HC; (A–F) SSI of specific ROIs under BC index; (G–H) SSI of specific ROIs under DC index; (I–J) SSI of specific ROIs under CC index; (K–L) SSI of specific ROIs under NE index.

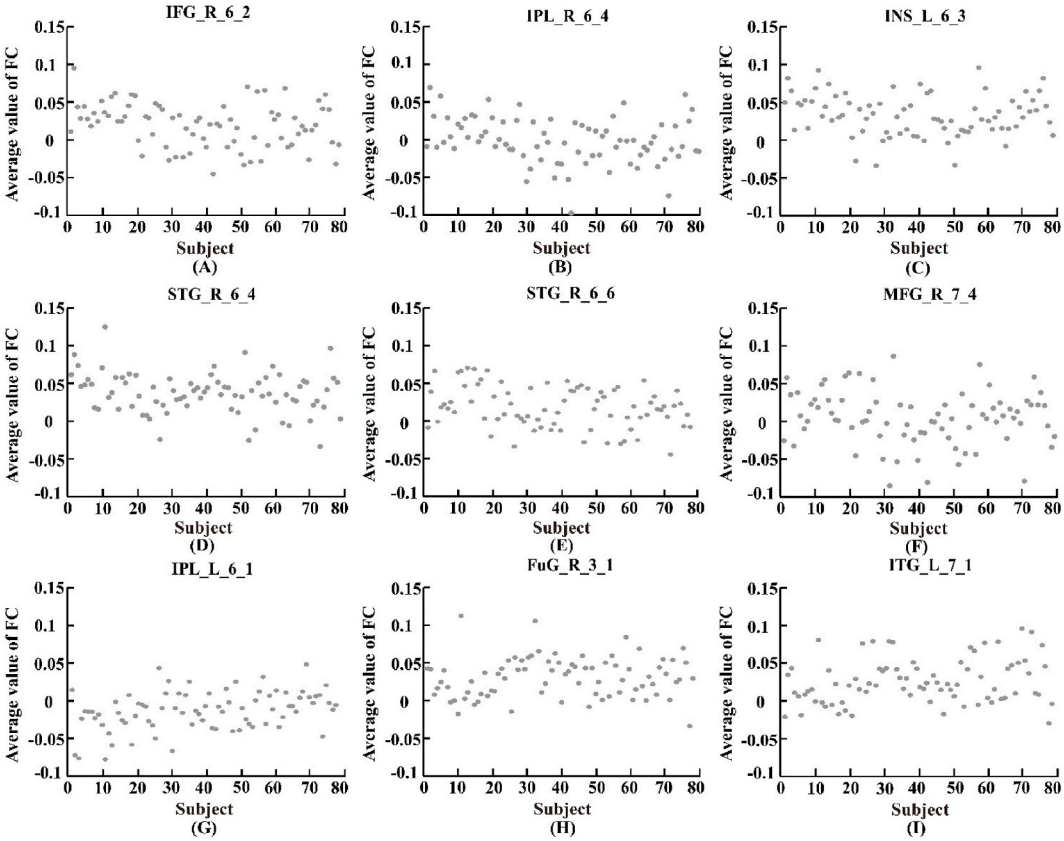

Fig. 5. Cluster of SSI values at the specific ROIs for NTLE and HC under the conventional FC model, the first 20 subjects are NTLE,and the last 60 subjects are HC. (A–I) SSI of specific ROIs under the conventional FC model.

Table 4
Classification accuracy and validation by 10 times random validation method.

Classification model	Accuracy/%	Sensitivity/%	Specificity/%	Area Under Curve/%
Network-level specific FC model	93.80	98.30	80.00	94.00
Conventional FC model	87.50	88.30	85.00	89.00

Table 5
Classification accuracy and validation by Hold-out.

Classification model	Accuracy/%	Area Under Curve/%	Training time/s	Precision/%
Network-level specific FC model	93.46	94.50	35.93	95.18
Conventional FC model	86.88	93.20	32.85	90.92

4.3. Limitations and prospects

The cause to employ three methods of feature extraction and a SVM with 2 validations including Hold-out method and 10 times random cross validation, mainly considered the small sample in this study. If there are a large number of samples, more advanced machine learning methods even deep learning methods should be considered carefully, because the Hold-out method is highly randomized and requires multiple random divisions and repeated experiments to take the average value. High-field MRI increases the resolution and, in several publications, was shown to improve the detection of focal cortical dysplasias and mild cortical malformations. For those cases without any tissue abnormality in neuroimaging, even at 7 T, scalp EEG alone is insufficient to delimitate the epileptogenic zone [35]. The detection of NTLE by MRI is incomplete. We use MRI technology to detect functional abnormalities in NTLE through a specific FC model, verifying that the specific FC model is superior to conventional models. The functional lesions in patients with temporal lobe epilepsy are not limited to the temporal lobe. Due to the limitations of current research on experimental subjects, we will conduct more studies on other types of epilepsy patients in the future. Meanwhile, we will collect data from PTLE

patients to further investigate the impact of structural damage in future experiments.

5. Conclusions

Considering the healthy people as a control, we constructed a network-level specific FC model, which can effectively screen the specific and unique functional imaging markers for NTLE. The specific regions including frontal lobe, temporal lobe, parietal lobe, hippocampus, and occipital lobe, Additionally, they could construct a good classifier for NTLE with great classification accuracy and stability, thus a specific NTLE classifier was constructed whose classification accuracy of 10 times random cross validation is 93.80 %, respectively, and the classification accuracy of hold-out method is 93.5 %,all significantly better than the performances of the conventional FC model of Pearson correlation. This study may provide a new method for accurate detection of functional biomarkers of NTLE by rfMRI, and may be helpful to clinical machine-assisted diagnosis.

CRediT authorship contribution statement

Xue Yang: Writing – original draft. **Manling Ge:** Writing – review & editing. **Shenghua Chen:** Writing – review & editing. **Kaiwei Wang:** Data curation. **Hao Cheng:** Data curation. **Zhiqiang Zhang:** Data curation.

Informed consent

Informed consent was obtained from all participants included in the study.

Ethics statement

The study was approved by the Biomedical Ethics Committee of Hebei University of Technology (Number: HEBUThMEC2021003) and the methods were carried out in accordance with the approved guidelines. All the subjects have been informed and signed informed consent before the experiments.

Funding

This work was financially supported by Graduate Student Innovation Funding Project of Hebei Province (No. CXZZSS2022040).

Declaration of competing interest

The authors declare the following financial interests/personal relationships which may be considered as potential competing interests: Reports a relationship with that includes:. Has patent pending to. If there are other authors, they declare that they have no known competing financial interests or personal relationships that could have appeared to influence the work reported in this paper.

Acknowledgements

The authors thanks funding and Yingxin Cao and Hao Cheng for their guidance and discussions throughout this research.

Data availability

The data presented in this study are available on request from the corresponding author.

References

[1] D.J. Englot, V.L. Morgan, C. Chang, Impaired vigilance networks in temporal lobe epilepsy: mechanisms and clinical implications, Epilepsia 61 (2) (2020) 189–202, https://doi.org/10.1111/epi.16423.
[2] C. LoPinto-Khoury, M.R. Sperling, C. Skidmore, M. Nei, J. Evans, A. Sharan, S. Mintzer, Surgical outcome in PET-positive, MRI-negative patients with temporal lobe epilepsy, Epilepsia 53 (2) (2012) 342–348, https://doi.org/10.1111/j.1528-1167.2011.03359.x.
[3] A.A. Cohen-Gadol, C.C. Bradley, A. Williamson, J.H. Kim, M. Westerveld, R.B. Duckrow, D.D. Spencer, Normal magnetic resonance imaging and medial temporal lobe epilepsy: the clinical syndrome of paradoxical temporal lobe epilepsy, J. Neurosurg. 102 (5) (2005) 902–909, https://doi.org/10.3171/jns.2005.102.5.0902.
[4] O. Hardiman, T. Burke, J. Phillips, S. Murphy, B. O'Moore, H. Staunton, M.A. Farrell, Microdysgenesis in resected temporal neocortex: incidence and clinical significance in focal epilepsy, Neurology 38 (7) (1988) 1041–1047, https://doi.org/10.1212/wnl.38.7.1041.
[5] É.L.M. Vieira, F.M.A. Martins, P.M.Q. Bellozi, A.P. Gonçalves, J.M. Siqueira, A. Gianetti, A.L. Teixeira, A.C.P. de Oliveira, PI3K, mTOR and GSK3 modulate cytokines' production in peripheral leukocyte in temporal lobe epilepsy, Neurosci. Lett. 756 (2021) 135948, https://doi.org/10.1016/j.neulet.2021.135948.
[6] R. Kuba, I. Tyrlíková, J. Chrastina, B. Slaná, M. Pažourková, J. Hemza, M. Brázdil, Z. Novák, M. Hermanová, I. Rektor, "MRI-negative PET-positive" temporal lobe epilepsy: invasive EEG findings, histopathology, and postoperative outcomes, Epilepsy Behav.: E&B 22 (3) (2011) 537–541, https://doi.org/10.1016/j.yebeh.2011.08.019.
[7] D.A. Lee, H.-J. Lee, H.C. Kim, K.M. Park, Temporal lobe epilepsy with or without hippocampal sclerosis: structural and functional connectivity using advanced MRI techniques, J. Neuroimaging 31 (5) (2021) 973–980, https://doi.org/10.1111/jon.12898.
[8] Olaf & Sporns, Graph theory methods: applications in brain networks, Dialogues Clin. Neurosci. (2018). Retrieved from, http://www.ncbi.nlm.nih.gov/pubmed/30250388.

[9] X. Wen, M. Yang, L. Hsu, D. Zhang, Test-retest reliability of modular-relevant analysis in brain functional network, Front. Neurosci. 16 (2022) 1000863, https://doi.org/10.3389/fnins.2022.1000863.
[10] V. Ives-Deliperi, J.T. Butler, Mechanisms of cognitive impairment in temporal lobe epilepsy: a systematic review of resting-state functional connectivity studies, Epilepsy Behav. 115 (2021) 107686, https://doi.org/10.1016/j.yebeh.2020.107686.
[11] R. Fruengel, T. Bröhl, T. Rings, K. Lehnertz, Reconfiguration of human evolving large-scale epileptic brain networks prior to seizures: an evaluation with node centralities, Sci. Rep. 10 (1) (2020) 21921, https://doi.org/10.1038/s41598-020-78899-7.
[12] H. Yang, J. Ren, Q. Wang, Abnormal Brain network in epilepsy and associated comorbidites, in: Neuropsychiatry, 8, 2018, https://doi.org/10.4172/Neuropsychiatry.1000429.
[13] C.P. Panayiotopoulos, The new ILAE report on terminology and concepts for organization of epileptic seizures: a clinician's critical view and contribution, Epilepsia 52 (12) (2011) 2155–2160, https://doi.org/10.1111/j.1528-1167.2011.03288.x.
[14] B.C. Bernhardt, L. Bonilha, D.W. Gross, Network analysis for a network disorder: the emerging role of graph theory in the study of epilepsy, Epilepsy Behav. 50 (2015) 162–170, https://doi.org/10.1016/j.yebeh.2015.06.005.
[15] X. Wang, T. Hu, Q. Yang, D. Jiao, Y. Yan, L. Liu, Graph-theory based degree centrality combined with machine learning algorithms can predict response to treatment with antiepileptic medications in children with epilepsy, J. Clin. Neurosci. 91 (2021) 276–282, https://doi.org/10.1016/j.jocn.2021.07.016.
[16] R.D. Bharath, R. Panda, J. Raj, S. Bhardwaj, S. Sinha, G. Chaitanya, K. Raghavendra, R.C. Mundlamuri, A. Arimappamagan, M.B. Rao, J. Rajeshwaran, K. Thennarasu, K.K. Majumdar, P. Satishchandra, T.K. Gandhi, Machine learning identifies "rsfMRI epilepsy networks" in temporal lobe epilepsy, Eur. Radiol. 29 (7) (2019) 3496–3505, https://doi.org/10.1007/s00330-019-5997-2.
[17] E.-N. Cheong, J.E. Park, D.E. Jung, W.H. Shim, Extrahippocampal radiomics analysis can potentially identify laterality in patients with MRI-negative temporal lobe epilepsy, Front. Neurol. 12 (2021) 706576, https://doi.org/10.3389/fneur.2021.706576.
[18] M. Jenkinson, C.F. Beckmann, T.E.J. Behrens, M.W. Woolrich, S.M. Smith, Fsl, Neuroimage 62 (2) (2012) 782–790, https://doi.org/10.1016/j.neuroimage.2011.09.015.
[19] M. Jenkinson, P. Bannister, M. Brady, S. Smith, Improved optimization for the robust and accurate linear registration and motion correction of brain images, Neuroimage 17 (2) (2002) 825–841, https://doi.org/10.1016/s1053-8119(02)91132-8.
[20] Y. Zhou, J. Tang, Y. Sun, W.F.Z. Yang, Y. Ma, Q. Wu, S. Chen, Q. Wang, Y. Hao, Y. Wang, M. Li, T. Liu, Y. Liao, A brainnetome atlas-based methamphetamine dependence identification using neighborhood component analysis and machine learning on functional MRI data, Front. Cell. Neurosci. 16 (2022) 958437, https://doi.org/10.3389/fncel.2022.958437.
[21] C.-G. Yan, X.-D. Wang, X.-N. Zuo, Y.-F. Zang, DPABI: data processing & analysis for (resting-state) brain imaging, Neuroinformatics 14 (3) (2016) 339–351, https://doi.org/10.1007/s12021-016-9299-4.
[22] O. Sporns, Graph theory methods: applications in brain networks, Dialogues Clin. Neurosci. 20 (2) (2018) 111–121, https://doi.org/10.31887/DCNS.2018.20.2/osporns.
[23] S. Amiri, J. Mehvari-Habibabadi, N. Mohammadi-Mobarakeh, S.S. Hashemi-Fesharaki, M.M. Mirbagheri, K. Elisevich, M.-R. Nazem-Zadeh, Graph theory application with functional connectivity to distinguish left from right temporal lobe epilepsy, Epilepsy Res. 167 (2020) 106449, https://doi.org/10.1016/j.eplepsyres.2020.106449.
[24] E.T. Bullmore, D.S. Bassett, Brain graphs: graphical models of the human brain connectome, Annu. Rev. Clin. Psychol. 7 (2011) 113–140, https://doi.org/10.1146/annurev-clinpsy-040510-143934.
[25] M.G. Hart, R.J.F. Ypma, R. Romero-Garcia, S.J. Price, J. Suckling, Graph theory analysis of complex brain networks: new concepts in brain mapping applied to neurosurgery, J. Neurosurg. 124 (6) (2016) 1665–1678, https://doi.org/10.3171/2015.4.JNS142683.
[26] E. Bullmore, O. Sporns, Complex brain networks: graph theoretical analysis of structural and functional systems, Nat. Rev. Neurosci. 10 (3) (2009) 186–198, https://doi.org/10.1038/nrn2575.
[27] H. Nazeer, N. Naseer, A. Mehboob, M.J. Khan, R.A. Khan, U.S. Khan, Y. Ayaz, Enhancing classification performance of fNIRS-BCI by identifying cortically active channels using the z-score method, Sensors 20 (23) (2020) 6995, https://doi.org/10.3390/s20236995.
[28] H. Shen, L. Wang, Y. Liu, D. Hu, Discriminative analysis of resting-state functional connectivity patterns of schizophrenia using low dimensional embedding of fMRI, Neuroimage 49 (4) (2010) 3110–3121, https://doi.org/10.1016/j.neuroimage.2009.11.011.
[29] J. Yang, J. Yang, D. Zhang, J. Lu, Feature fusion: parallel strategy vs. serial strategy, Pattern Recogn. 36 (6) (2003) 1369–1381, https://doi.org/10.1016/S0031-3203(02)00262-5.
[30] S. Chen, Z. Fang, S. Lu, C. Gao, Efficacy of regularized multitask learning based on SVM models, IEEE Trans. Cybern. (2022), https://doi.org/10.1109/TCYB.2022.3196308.
[31] S. Wang, L.J. Tepfer, A.A. Taren, D.V. Smith, Functional parcellation of the default mode network: a large-scale meta-analysis, Sci. Rep. 10 (1) (2020) 16096, https://doi.org/10.1038/s41598-020-72317-8.
[32] G. Hwang, K. Dabbs, L. Conant, V.A. Nair, J. Mathis, D.N. Almane, A. Nencka, R. Birn, C. Humphries, M. Raghavan, E.A. DeYoe, A.F. Struck, R. Maganti, J. R. Binder, E. Meyerand, V. Prabhakaran, B. Hermann, Cognitive slowing and its underlying neurobiology in temporal lobe epilepsy, Cortex 117 (2019) 41–52, https://doi.org/10.1016/j.cortex.2019.02.022.
[33] F. Brigo, Contralateral knee sign: an extension of the Hoover's sign to unveil functional paralysis of knee extension, Neurol. Sci. 44 (9) (2023) 3351–3352, https://doi.org/10.1007/s10072-023-06852-3.
[34] S. Gates, D.E. Hackman, N. Agarwal, W. Zhang, P. Barnard, J.R. White, Postoperative neurologic outcome in patients undergoing resective surgery for parietal lobe epilepsy: a systematic review, Neurology 102 (12) (2024) e209322, https://doi.org/10.1212/WNL.0000000000209322.
[35] R.L. Saute, J.E. Peixoto-Santos, T.R. Velasco, J.P. Leite, Improving surgical outcome with electric source imaging and high field magnetic resonance imaging, Seizure 90 (2021) 145–154, https://doi.org/10.1016/j.seizure.2021.02.006.